FIELD ELECTRON EMISSION PERFORMANCE AND ORTHODOXY TEST OF TUNGSTEN EMITTERS WITH AND WITHOUT THIN TUNGSTEN TRIOXIDE BARRIER

Daniel Burda

Doctoral Degree Programme (1), FEEC BUT

E-mail: xburda14@stud.feec.vutbr.cz

Supervised by: Dinara Sobola

E-mail: sobola@feec.vutbr.cz

Abstract: This initial study aims to explore the topic of thin barrier layers for single tip cold field emitters. The experiment and measurements have been conducted in ultra-high vacuum field electron microscope. Additionally, micrographs of the emitter were obtained using scanning electron microscope. The performance of the emitter was evaluated using orthodoxy test and Murphy-Good plots, which can give more complete picture of emitter changes during field emission.

Keywords: Cold field emission, single tip field emitters, tungsten tip, self-heating of electron emitter, tungsten trioxide, dielectric barrier, Murphy-Good plot

1 INTRODUCTION

The research on the topic of field electron emission sources is motivated by many practical applications, which ranges from electron guns operating at room temperature, compact X-ray sources to novel field emission displays. Two main categories have emerged over the years, single tip field emitters (STFEs) and large area field emitters (LAFEs), usually consisting of many emission sites, for example arrays or clusters of nanorods or nanotubes. This paper deals with the former group of field emitters. The material mainly used for STFEs is tungsten due to its durability, high melting point, low sputtering ratio, the main applied research goals are to increase stability, emission current density, brightness, while also improve the longevity.

In cold field electron (CFE) emission regime, most of the electrons escape by tunneling from electron states below the Fermi level. An equation describing CFE from ideal planar metallic surfaces was published in 1956 by Good et al. [1], which since then has been modified and extended and used for analysis of CFE current–voltage (*I*–*V*) characteristics of various emitters not only the metallic. This approach may not be always phenomenological or mathematically correct but may still be "good enough" approximation. Recently, an orthodox CFE emitter test [2] for measured *I*–*V* characteristics to indicate, whether CFE theory can be used to describe an emitter properly and orthodox conditions [3] was developed.

The family of equations starting with the one in 1956 is called *Fowler-Nordheim equations*. Tunneling is assumed through *Schottky-Nordheim* (SN) barrier, which is illustrated in the Figure 1. Directly measured *I*–*V* characteristics from field electron microscope (FEM) can be used under specific *orthodox* conditions to extract emitter performance related properties. In this paper, *extended Murphy-Good equation* (EMG) is employed (more details on the subject in [2,3,4,5]):

$$I(V) = \{A^{\mathrm{SN}}(\theta \exp \eta) V_{\mathrm{R}}^{-\kappa}\} V^{\kappa} \exp(-\eta V_{\mathrm{R}}/V) \qquad (1)$$

where A^{SN} is the formal emission area assuming SN barrier tunneling, V_{R} is a (constant) reference measured voltage [4] needed to pull the top of a characteristic SN barrier, of zero-field height φ, down to the emitter Fermi level [2], θ and η are work function dependent scaling parameters defined

in [4], $\eta \sim 9.836239\ (\mathrm{eV}/\varphi)^{1/2}$, parameter $\kappa(\eta)$ is also related: $\kappa = 2 - \eta/6$. By applying natural logarithm to (1), the equation becomes:

$$\ln\{I/V^{\kappa}\} = \ln\{A^{\mathrm{SN}}(\theta \exp\eta)V_{\mathrm{R}}^{-\kappa}\}V^{\kappa} - \eta V_{\mathrm{R}}/V \qquad (2)$$

The equation (2), called *theoretical Murphy-Good plot,* is linear as every parameter on its right side is constant except for *1/V*. For orthodox field emitters, it is possible to extract the emitter characteristic voltage conversion length (VCL) ζ_{C} and related [4] field enhancement factor γ and formal emission area A^{SN} by transforming measured characteristics into $\ln\{I/V^{\kappa}\}$ vs. $(1/V)$ and fitting it with a linear function [3]. When the transformed *I–V* characteristics cannot be fitted with linear function, it is an indicator of non-orthodox behavior and field emission related parameters cannot be extracted. The *electron emission convention* is used, which omits negative signs in electric fields, voltages, currents, and current densities and treats them as positive.

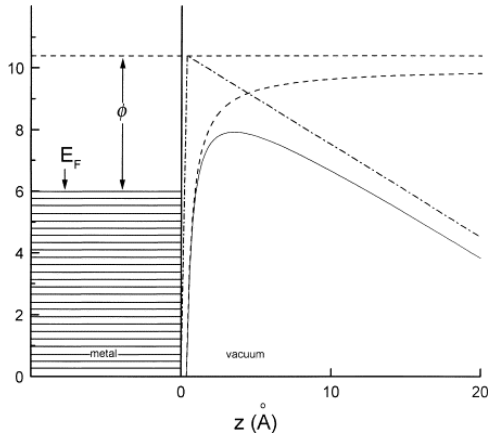

Figure 1: Representation of a metal-vacuum interface, E_{f} Fermi level, φ work function, dot-dash – triangular barrier, dashed line – image potential, full line – *Schottky-Nordheim barrier*. From [6].

2 EXPERIMENTAL CONDITIONS

The preparation and characterization of the electron emitter can be described in three phases. In the first phase, tungsten wire (GoodFellow no. 7440-33-7, 99.9+%) with diameter of 0.3 mm was electrochemically etched in in-house setup described elsewhere [7], which was configured for simple one-step lamellae drop-off technique. The etching of tungsten wire takes place in a thin lamella of 2M NaOH solution stretched out on a Pt ring, where the tungsten wire acts as the anode, and Pt ring acts as the cathode, detailed description can be found in [8,9]. With this etching technique, sharp tungsten tips with tip radius of 50 nm and less can be prepared, which makes them suitable for field electron emission applications. After the etching in NaOH solution the produced tungsten tip is inevitably covered with thin layers of WO_X and ternary-phase oxides [10].

In the second phase, the tungsten tip was loaded into in-house FEM for subsequent cleaning of the tungsten tip by self-sputtering and then the measurement of field electron emission characteristics and field emission pattern of the clean tungsten tip. During these steps, FEM was continuously pumped down to ultra-high vacuum (UHV) levels up to 10^{-7} Pa. The applied cathode voltage was set by Delong Instruments high voltage supply. The emission current between the tungsten emitter and Al coated Nd:YAG scintillator was measured by Keithley 485 Pico ammeter.

In the third phase, high cathode voltage was applied to the tungsten tip, which resulted in heating up of the tip by high current density. The temperature of the apex may reach up to over 1300 K, the emission shifts from field to field-thermal. After 5 minutes, the applied voltage, also the emission was switched off, and oxygen from a small attached cylinder was introduced into the FEM chamber through a precise needle valve, effectively increasing the pressure from $3.7 \cdot 10^{-7}$ Pa to $1 \cdot 10^{-5}$ Pa. After 2 minutes, the oxygen flow was stopped and the chamber was left to pump down for 4 hours until the initial pressure was restored. The formation of nanometer thin layer of high quality WO_3 on

the clean surface is assumed. The measured *I–V* characteristics of clean emitter and oxidized tungsten emitter are presented in the Figure 2.

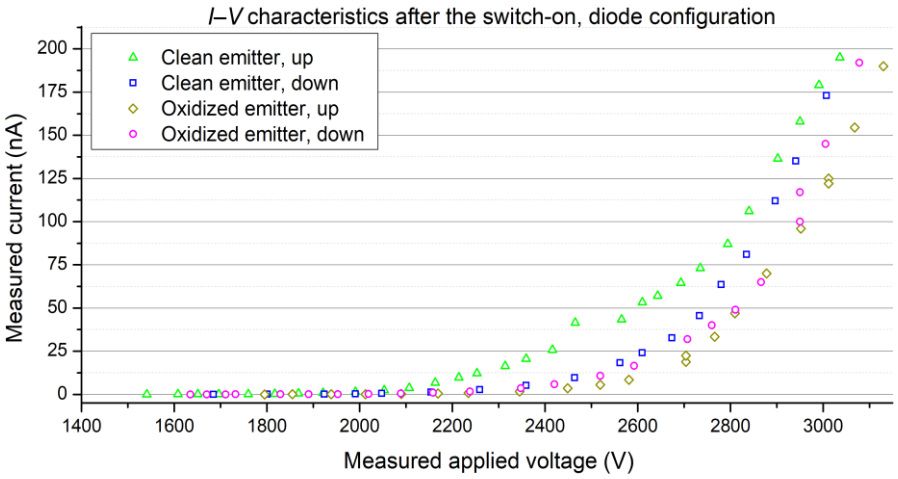

Figure 2: The emission characteristics of clean and oxidized tungsten emitter, forward (up) and backward (down) voltage scanning.

3 RESULTS

The work function of tungsten and WO_3 is assumed to be 4.5 eV and 5.6 eV respectively. Although the formation of WO_3 could not be observed directly, after the supposed oxidation of the apex of the emitter, the threshold voltage needed for stable emission current > 2 nA shifted significantly from the value of 2030 V for clean emitter to 2350 V, when the forward voltage scanning was performed (up). But during backward voltage scanning (down), the threshold voltage of oxidized emitter decreased and was of similar value: 2050 V (clean) and 2070 V (oxidized). This behavior indicates the surface changes on the apex of oxidized emitter during measurement steps. Recorded emission patterns are illustrated in the Figure 3, the main observable difference is in the brightness of the patterns, the change of emission centers is not noticeable. Accurate evaluation of changes over time in emission centers would require setup adjustments and is considered in the future.

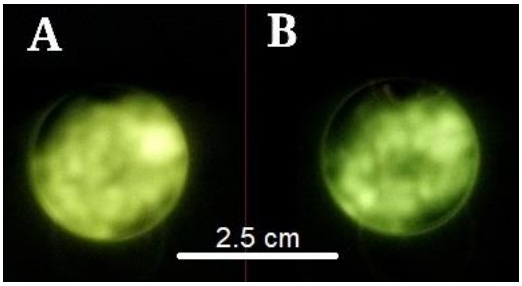

Figure 3: Comparison of the electron pattern projected at the backside of the scintillator. Applied cathode voltage of 3 kV (maximum measurement value). A) clean emitter, higher intensity/higher current observed B) supposedly oxidized emitter.

From the Murphy-Good plots presented in the Figure 4, the clean emitter shows clearly non-orthodox behavior in the left upper part of M-G plot for upward voltage increase, there may be several causes [3] including field-dependent geometry, heating-dependent changes in work function, absorbate removal and the tip can no longer be described by *Fowler-Nordheim theory*. The extracted data of interest are in Table 1, note the significant difference in A^{SN} by the factor of 7 between the spurious and the correct values. The non-spurious values are in good agreement with those of a conventional

< 100 nm radius tungsten tip. In the first three steps (excluding spurious part), the extracted parameters show a small progress, which may be attributed to the gradual tip blunting. The thickness of tungsten trioxide deposited during the third step is assumed to be several nanometers, because the difference between the values of A^{SN}, ζ_C, γ before and after the oxidization would be more significant otherwise.

Emitter, Step	*Orthodoxy test*	A^{SN} (nm^2)	ζ_C (m)	γ (-)
Clean, Up (spurious)	Undecided/Fail	1.01	$4.32 \cdot 10^{-7}$	$2.32 \cdot 10^{4}$
Clean, Up,	Pass	7.44	$4.89 \cdot 10^{-7}$	$2.05 \cdot 10^{4}$
Clean, Down	Pass	7.98	$5.39 \cdot 10^{-7}$	$1.85 \cdot 10^{4}$
Oxidized, Up	Pass	9.41	$5.51 \cdot 10^{-7}$	$1.81 \cdot 10^{4}$
Oxidized, Down	Pass	24.29	$6.002 \cdot 10^{-7}$	$1.665 \cdot 10^{4}$

Table 1: Emitter orthodoxy test results and field emission values: formal emission area A^{SN}, voltage conversion length ζ_C, field enhancement factor γ, calculated from plots in Figure 4.

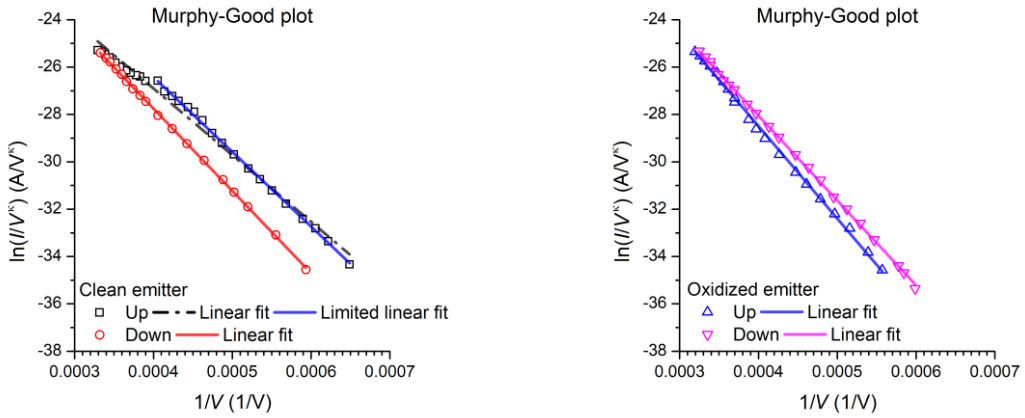

Figure 4: Murphy-Good plots and linear fits. Note the dash-dot black line – the example of improper fit leading to spurious results.

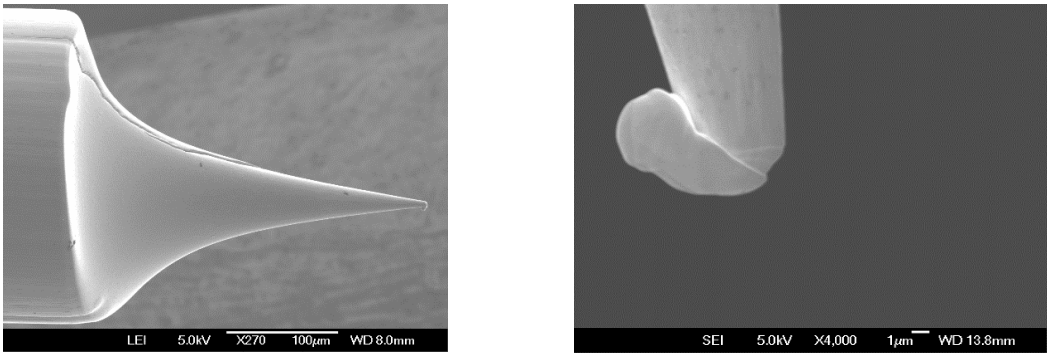

Figure 5: SEM micrographs of the examined emitter. The detail shows destruction of the apex.

After the FEM experiment, analysis using SEM revealed the destruction of the emitter apex, which is shown in the Figure 5. This phenomenon is common when the cold field emission regime changes towards thermal regime, which drains electrons even more towards the anode, resulting in rapid heating and melting.

Counterintuitively, it may not result in a significant change of the emission current. It is largely controlled by applied cathode voltage but also the setup conditions and the occurrence cannot be completely predicted. The values extracted from the M-G plots also give information, when the apex

of the emitter started to melt. It was most probably at the maximum applied voltage of 3 kV, between forward and backward voltage screening of the oxidized emitter. Then, during the backward voltage screening, the formal emission area increased by the factor of 2.5 and the tip became more blunter as indicated by the larger further decrease of extracted field enhancement factor.

4 SUMMARY

During the FEM measurements, several changes indicating modifications of the field emitter were observed. The method of oxidation was proposed and demonstrated. The thickness of prepared tungsten trioxide barrier on top of the tungsten emitter tip was assumed to be of several nanometers thick only. More experiments aimed towards preparation of tungsten trioxide barriers with a thickness larger than 10 nm are to be carried out in the future.

After the oxidization, at applied cathode voltage of 3 kV, the emitter started to melt, which became evident only after the subsequent SEM imaging. During this event, the formal emission area increased by the factor of 2.5. Whether the tungsten trioxide layer have survived the melting is unclear and superfluous, it can no longer be analyzed for field emission. In the follow-up experiments detailed element analysis with TEM to clarify the formation of tungsten trioxide layer is planned.

ACKNOWLEDGEMENT

The author would like to thank to EBL group at Institute of Scientific Instruments of the Czech Academy of Sciences, where the presented research was conducted, the infrastructure was supported by RVO:68081731. The work was also supported by FEKT-S-20-6352.

REFERENCES

[1] GOOD, R H. and Erwin W. MÜLLER. 1956. Field Emission. *J Vac Sci Technol B* [online]. Berlin, Heidelberg: Springer Berlin Heidelberg, 176–231.

[2] ALLHAM, Mohammad, Richard FORBES, Alexandr KNÁPEK, Marwan MOUSSA. 2020. Implementation of the Orthodoxy Test as a Validity Check on Experimental Field Emission Data. *J Elect Eng Technol* [online]. **71**.

[3] FORBES, Richard G. 2018. Tutorial lecture, April 2018: Field electron emission and the interpretation of Fowler-Nordheim plots. [online]. DOI: 10.13140/RG.2.2.13535.15526/

[4] FORBES, Richard G. 2019. The Murphy–Good plot: a better method of analysing field emission data. *Roy Soc Open Sci* [online]. **6**(12).

[5] FORBES, Richard G and Jonathan H.B DEANE. 2007. Reformulation of the standard theory of Fowler–Nordheim tunnelling and cold field electron emission. *P Roy Soc A-Math Phy* [online]. **463**(2087), 2907–2927.

[6] MODINOS, A. 2001. Theoretical analysis of field emission data. *Solid State Electron* [online]. **45**(6), 809–816.

[7] KNÁPEK, Alexandr, Jiří SÝKORA, Jana CHLUMSKÁ and Dinara SOBOLA. 2017. Programmable set-up for electrochemical preparation of STM tips and ultra-sharp field emission cathodes. *Microelectron Eng* [online]. **173**, 42–47.

[8] MELMED, Allan J. 1998. The art and science and other aspects of making sharp tips [online]. *J Vac Sci Technol B* [online]. **9**(2).

[9] KLEIN, M. and G. SCHWITZGEBEL. 1997. An improved lamellae drop-off technique for sharp tip preparation in scanning tunneling microscopy. *Rev Sci Instrum*. **68**(8), 3099–3103.

[10] KNÁPEK, Alexandr. 2013. Methods of preparation and characterization of experimental field-emission cathodes. Brno. Doctoral thesis. Brno University of technology.